Building and Environment 207 (2022) 108528

Contents lists available at ScienceDirect

Building and Environment

journal homepage: www.elsevier.com/locate/buildenv

# Impact of atmospherical stability and intra-hour variation of meteorological data in the variability of building air change rates

Vitor E.M. Cardoso [a,*], M. Lurdes Simões [a], Nuno M.M. Ramos [a], Ricardo M.S.F. Almeida [a,b], Manuela Almeida [c], Lígia Conceição [d]

[a] CONSTRUCT-LFC, Department of Civil Engineering, Faculty of Engineering, University of Porto, 4200-465, Porto, Portugal
[b] Polytechnic Institute of Viseu, School of Technology and Management, Department of Civil Engineering, Campus Politécnico de Repeses, 3504-510, Viseu, Portugal
[c] ISISE, Department of Civil Engineering (DEC), School of Engineering, University of Minho, Campus de Azurém, Guimarães, 4800-058, Portugal
[d] Research Center for Territory, Transports and Environment (CITTA), Department of Civil Engineering, Faculty of Engineering, University of Porto, 4200-465, Porto, Portugal

ARTICLE INFO

*Keywords:*
Air infiltration
Meteorological data
Airtightness
Air change rate
Atmospheric stability
Wind shear coefficient

ABSTRACT

In contrast with structural engineering, where the focus for design is on extreme values, for the proper assessment and modelling of air change rates in natural ventilation and infiltration, one must use the full range of input variables. Most of the modelling in infiltration research relies on hourly datasets for air infiltration balance. This consideration overlooks the intra-hour variability on meteorological variables. Additionally, it is customary to assume unchanging neutral atmospheric conditions when modelling, which affects the calculated airflows. This work intends to detail and quantify these effects in a case study representative of an average single-family dwelling in a Southern European climate setup. By comparing four setups with an increasing degree of complexity, a median of 0.04 $h^{-1}$ of the hourly standard deviations in air change rates (ACH) is attributed to the time step effect. Approximately 43% of the occurrences experienced non-neutral atmospheric stability, skewing for stable conditions. This effect contributed to differences in the ACHs ranging from −0.202 to 0.131 $h^{-1}$ at the 5% and 95% quantiles. Overall, by using hourly uniform distributions and smart sampling of meteorological variables, one ensures that the values in between and others potentially occurring around the boundaries are being considered for air change rates calculation, and therefore providing a more detailed picture of actual conditions.

*Symbol Description Unit*

| | | |
|---|---|---|
| $ELA_{50}$ | Effective leakage area at a pressure difference of 50 Pa | $m^2$ |
| $Q_{50}$ | Airflow volume at a pressure difference of 50 Pa | $m^3/h$ |
| $C_{D50}$ | Discharge coefficient at a pressure difference of 50 Pa | - |
| $\rho$ | Air density | $kg/m^3$ |
| $n_{50}$ | Air change rate at a pressure difference of 50 Pa | $m^3/h$ |
| $q_{50}$ | Envelope air permeability at a pressure difference of 50 Pa | $m^3/h{\cdot}m^2$ |
| $A_{env}$ | Envelope area | $m^2$ |
| $Q_{\Delta Pi}$ | Airflow volume at $\Delta P$ pressure difference at the $i$ surface | $m^3/s$ |
| $C$ | Airflow coefficient | $m^3/(h{\cdot}Pa^n)$ |
| $\Delta P_i$ | Pressure difference at the $i$ surface | Pa |
| n | Airflow exponent | - |
| $\Delta P_{wi}$ | Pressure difference resulting from the wind effect at the $i$ surface | Pa |
| $\Delta P_{si}$ | Pressure difference resulting from the stack effect at the $i$ surface | Pa |
| IRP | Internal reference pressure | Pa |
| $p_{ref}$ | Reference atmospheric pressure (at 293.15 K) | kPa |
| $M$ | Molar mass of dry air | kg/mol |
| R | Universal gas constant | J/(mol•K) |
| $T_{ext}$ | Exterior temperature | K |
| $C_{p_i}$ | Wind pressure coefficient (Cp) at the $i$ surface | - |
| $v_{10}$ | Wind speed at a height of 10 m | m/s |
| $\delta_{met}$ | Thickness of the atmospheric boundary layer at the location of the meteorological station | m |
| $H_{met}$ | Height of the meteorological station | m |
| $\alpha_{met}$ | Wind shear coefficient at the location of the meteorological station | - |

* Corresponding author.
*E-mail address:* v.cardoso@fe.up.pt (V.E.M. Cardoso).

https://doi.org/10.1016/j.buildenv.2021.108528
Received 16 June 2021; Received in revised form 26 October 2021; Accepted 28 October 2021
Available online 3 November 2021

| | |
|---|---|
| $H_i$ | Height of surface i of the envelope m |
| $\delta$ | Thickness of the atmospheric boundary layer at the location of the dwelling m |
| $\alpha$ | Wind shear coefficient (WSC) - |
| $h_{mean,i}$ | Mean height of the *i* surface m |
| $h_{max}$ | Height of the highest surface or interface m |
| $T_{int}$ | Interior temperature K |
| $A_{envi}$ | Envelope area of the *i* surface $m^2$ |
| V | Volume of the dwelling $m^3$ |
| ACH | Air change rate $h^{-1}$ |
| $\sigma_{WD}$ | Standard deviation of the horizontal component of the wind direction at a particular hour deg |
| $s_a$ | Average of the sines of the wind angle readings at a particular hour rad |
| $c_a$ | Average of the cosines of the wind angle readings at a particular hour rad |
| $\theta_i$ | Wind angle reading at time i deg |

## 1. Introduction

### 1.1. Natural variability of air change rates

Climate and meteorological variability is a key aspect for the assessment of the potential of numerous technologies that add value to society [1–3]. This approach is particularly important when dealing with the energy performance of buildings since most systems, especially passive ones, are highly reliant on environmental conditions [4]. Air infiltration through the building envelope is an obvious example of a time-variable property.

Together with ventilation, the produced airflow influences the quality of the indoor environment by regulating pollutants concentrations, the comfort of occupants, and heat and moisture transfer [5,6]. Air infiltration is further influenced by the physical properties and durability of building materials [7,8]. While controlling the maximum concentration of indoor air pollutants demands a minimum threshold of fresh airflow, optimizing the energy performance implies an upper limit of the building air change rate (ACH). Many south European existing buildings still rely on natural ventilation, usually combining stack ducts and a leaky envelope [9].

Naturally induced air change rates in buildings depend on several factors, which can be grouped into two main categories: dwelling related characteristics, i.e., envelope airtightness, position and number of openings, building/dwelling height, roof slope, aspect ratio, orientation, number of facades exposed, etc.; and terrain and meteorological data, i.e., terrain roughness, wind direction, wind speed, and air temperature offset between the indoors and outdoors, among others [10].

Regarding meteorological variables, Building Energy Simulation (BES) and Airflow Network (AFN) software are often used with 1-h readings or averages to compute airflow balances [11–13]. However, large time steps between readings can result in loss of information since the variability in the meantime is ignored, which is particularly important for wind direction and speed. Existing studies have already shown the importance of the time-interval when it comes to calculation of air infiltration in real conditions [14,15].

Additionally, in the in-between, other parameters such as wind shear coefficients and pressure coefficients, which have a significant effect on the air change rates, suffer by similar simplifications.

The wind shear coefficient (α or WSC), or vertical wind profile exponent, is used to convert measured wind speeds to estimated ones at different heights. Wind shear is dependent on atmospheric stability, surface roughness and height [16,17]. As atmospheric stability is dynamic over time, so is the wind shear coefficient. Still, in most BES and AFN models, the wind shear coefficient is often assumed to depend only on terrain conditions and thus is considered constant over time, i.e., taking neutral atmospheric stability. The AIM-2 model is an exception, as it considers two atmospheric stability classes in the input [18]. Despite the widespread use of this simplification, previous research shows monthly average variations up to 64% from summer to winter months [19] and even higher offsets in intraday variations [20].

The literature review shows that this can significantly impact the resulting air change rates [21]. Using fixed or variable exponents results in differences up to 1.24 times on ventilation airflows and 1.12 times on modelling energy saving potentials. Moreover, both under and over estimation of ventilation performance were recorded in different periods of the day. Overall, the differences found indicate that the simplification of considering a single atmospheric stability can have an impact as high as that of wind pressure coefficients simplifications [22] since, as the first impact the latter, there is a cumulative effect.

Wind pressure coefficients (Cp or WPC) result from the relation between the static and the dynamic pressures exerted by air density, wind speed and direction in a given point of the exposed building envelope. This balance also depends on the on-site conditions and building geometry [23].

Pressure coefficients are one of the variables inducing higher degrees of uncertainty in modelled airflows [24,25].

Accuracy issues occur across different positions in a single façade [26] and in a single position along time [27]. For simulation purposes, the surface average is often used as input. However, air change rates calculated based on local coefficients oscillated between 0.23 and 5.07 times the ones calculated with surface averages [28].

Although possible, full-scale field measurement of the wind pressure coefficients requires considerable resources and is a time-consuming task [29]. Most of the available data used in simulation come from wind tunnel studies on building models [30] or numerical models constructed on parametrical analysis of the first [31].

Due to the high number of influencing factors, obtaining reliable input data for simulation is constrained by the scope and extension of the developed studies [31]. Different models based on separate data sources, although modelling the same building and theoretical conditions, present variations up to 40% on exposed structures, and up to 100% in sheltered ones [25].

In the latest efforts, using some of the most recent highly detailed wind tunnel data [32], the use of established methods in the research area and new ones for the development of analytical models is providing prediction tools with higher degrees of accuracy [33–35]. These recent advances are closely fitting the input data they are generated from and therefore may not represent some factors combination, particularly concerning the impact of wind speed profile exponents in the spectrum of wind pressure coefficients.

### 1.2. Gaps and objectives

The literature review shows that using hourly averaged meteorological data and wind shear and wind pressure coefficients dependent only on terrain characteristics may overlook variations in the overall air change rates. As one intends to maintain the ACH in a narrow range, a more detailed knowledge of its variability may provide ground for better design of natural ventilation systems.

One example is the possibility to include inflexions that wind pressure coefficients experience as angle incidence travels the 360° range,

which may be disregarded in a simplified approach.

Contemplating these issues, the main objective of the present work is to propose and present an increasingly comprehensive methodology for the modelling of the intra-hour variation of air change rates, including the effect of changing atmospheric stability. To that end, it is necessary to quantify and compare the impact, in intermediate outputs and air change rates, of:

- Including meteorological variability in the quantification of wind shear coefficients, in contrast with only terrain dependent ones;
- Using 10-min readings of meteorological variables, in contrast with hourly readings or averages;
- Implementing the stochastic nature of meteorological variables, in contrast with averaged input.

## 2. Methodology

### 2.1. Airflow rates

A numerical single-zone model of a single-family dwelling with natural ventilation, combining stack ducts and a leaky envelope, was developed to pursue the objectives. It was then used to simulate different scenarios of a simulation campaign. Fig. 1 shows a schematic representation of the model, where the exposed surface areas of a two-story dwelling are parametrized, and the respective input data required to calculate air change rates is described.

The first number in the nomenclature of each envelope surface refers to: 1 – windward wall; 2 – leeward wall; 3 – wall to the right of the windward wall (clockwise); 4 – wall to the left of the leeward wall (counterclockwise), in accordance with AIVC documentation [36]. L1 and L2 refer to the lower and upper halves of the ground floor, respectively. U1 and U2 refer to the lower and upper halves of the first floor, respectively. Surfaces 5 and 6 refer to the two halves of the roof, and V-1, V-2 to the duct connecting to the ground and first floor, in the same order.

The process here presented for airflow convergence has the same architecture of the iterative method of EN 15242:2007 [37], transposed as method 1 in the standard EN 16798-7:2017 [38]. The modelling of the airflow paths is based on one-way power laws for the volume flow ($Q = C{\cdot}\Delta P^{n}$) and the calculation of Eqs. (1)–(8), following an iterative process for the airflow convergence. The power law is the equation adopted in most international standards regarding airtightness testing. Additionally, experimental campaigns suggest that the power law produces better results than the quadratic law at lower pressures [39,40]. The formulation background is available in ASHRAE documentation [41].

As computed in Eqs. (1)–(3), the airflow coefficient (C) can be expressed as a function of air permeability, envelope area, pressure differential at which the air permeability was measured, and airflow exponent. The use of the air permeability rate ($q_{50}$) instead of the air change rate ($n_{50}$) allows establishing a relationship between airtightness performance and envelope surface areas (Eq. (3)). For each exposed surface, the airflow is calculated (Eq. (3)).

$$ELA_{50} = \frac{Q_{50}}{C_{D50}}\sqrt{\frac{\rho}{2{\cdot}50}} \tag{1}$$

$$Q_{50} = q_{50}\,A_{env} \tag{2}$$

$$Q_{\Delta Pi} = C(\Delta P_i)^n = C_{D50}\,ELA_{50}\sqrt{\frac{2{\cdot}50}{\rho}}\left(\frac{\Delta P_i}{50}\right)^n = Q_{50i}\left(\frac{\Delta P_i}{50}\right)^n = \frac{q_{50}A_{envi}}{50^n}\Delta P_i{}^n \tag{3}$$

The pressure difference in each surface ($\Delta P_i$) is computed from Equation (6)), which, besides the wind (Eq. (4)) and stack (Eq. (5)) effects, also includes the internal reference pressure (IRP), required to guarantee the convergence in the airflow volume.

$$\Delta P_{wi} = \frac{\frac{p_{ref}{\cdot}M}{R}}{2{\cdot}T_{ext}}C_{p_i}\left(v_{10}\left(\frac{\delta_{met}}{H_{met}}\right)^{\alpha_{met}}\left(\frac{H_i}{\delta}\right)^{\alpha}\right)^2 = \frac{176.49}{T_{ext}}C_{p_i}\left(v_{10}\left(\frac{\delta_{met}}{H_{met}}\right)^{\alpha_{met}}\left(\frac{H_i}{\delta}\right)^{\alpha}\right)^2 \tag{4}$$

$$\Delta P_{si} = -\,9.81\left(h_{mean,i} - h_{max}\right)\frac{p_{ref}{\cdot}M}{R}\left(\frac{1}{T_{ext}} - \frac{1}{T_{int}}\right) = -\,9.81\left(h_{mean,i} - h_{max}\right)352.98\left(\frac{1}{T_{ext}} - \frac{1}{T_{int}}\right) \tag{5}$$

$$\Delta P_i = \Delta P_{wi} + \Delta P_{si} + IRP \tag{6}$$

Replacing Equation (6) into Equation (3) one obtains the air flow at each surface (Eq. (7)). For each time step, the ACH is the sum of either the positive, from outdoor to indoor, or the negative, from indoor to outdoor, surface air flows divided by the dwelling interior volume (Eq. (8)).

$$Q_{\Delta Pi} = C(\Delta P_i)^n = \frac{q_{50}A_{envi}}{50^n}(\Delta P_{wi} - \Delta P_{si} - IRP)^n \tag{7}$$

$$\sum Q_{\Delta Pi} = 0\,,\ for\ Q_{\Delta Pi} > 0\ \cup\ Q_{\Delta Pi} < 0\ : ACH = \frac{\sum Q_{\Delta Pi}}{V} \tag{8}$$

The use of the developed model requires that several assumptions are made. Most of these are often adopted or available as an option in airflow analysis software [12,13]. They are as follows:

- internal partitions and furniture are ignored;
- as rarely each single component is addressed solely when measurements are performed, the contribution of each of them to the whole building airtightness is unknown, and therefore, the air permeability is uniformly distributed along the exposed surfaces. This is a feature often available in airflow analysis software [12,13];
- each vertical exposed surface is horizontally divided in half, in each floor, to better identify possible changes in the flow direction, ease the pairing of wall sections with available WPCs, and overall, increase the detailing, consequently, the $h_{mean}$ of each wall section of the envelope walls occurs at an elevation of 25% and 75% of the ceiling height (Fig. 1), as these correspond to the mid height of each of the parametrized sections;
- the atmospheric pressure is considered to be of 101.325 kPa, and dry air is assumed when considering air densities. As temperature differences are already taken into account, a change from 0% to 100% relative humidity has residual impact in air density, i.e., at a temperature of 293.15 K it corresponds to a change of 0.84% in the air density, at 283.15 K, the change in air density is of 0.48% and at, 273.15 K it is reduced to 0.23%. The air density ratios at different atmospheric pressures, when a 10 K range (indoor-outdoor) of temperature is considered, if one considers the ranges between 97.000 kPa and 101.325 kPa, and between 101.325 kPa and

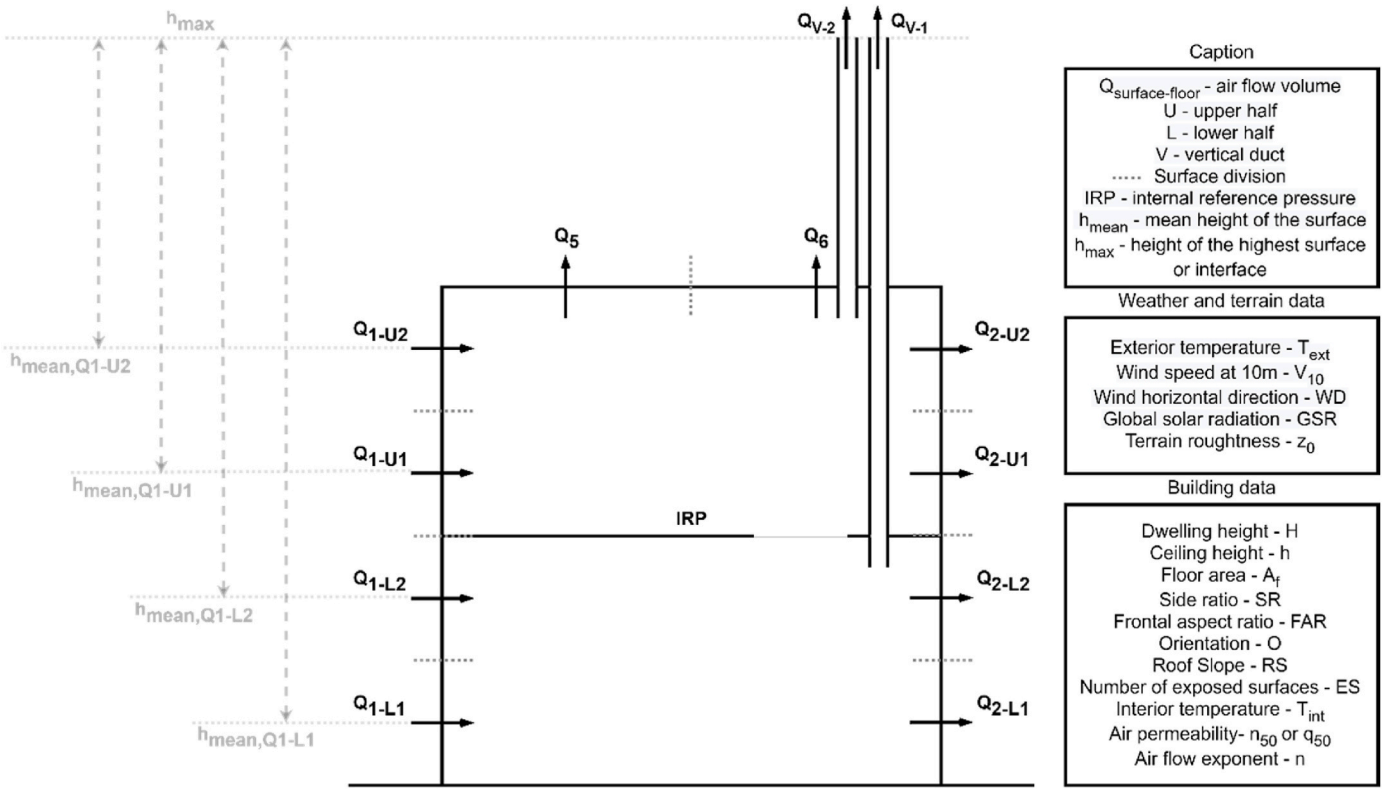


**Fig. 1.** Schematic profile of the parametrized exposed surface areas and respective required input data.

104.000 kPa, respectively, result in 0.0768% and 0.0144% discrepancies in comparison with static atmospheric pressure. These lower and upper limits portray the boundaries between which the atmospheric pressure at sea level usually varies;

- the IRP found at convergence corresponds to the internal pressure at the chosen height for the combination of natural forces at that moment.

### 2.2. Setups and data modelling

The meteorological data used in the present study was measured at the Porto/Pedras Rubras weather station, near Sá Carneiro Airport, in the northern region of Portugal. The station is located at a latitude of 41.2335, a longitude of −8.68133 and an altitude of 63 m. It is part of a broader governmental network of the Portuguese Institute for Sea and Atmosphere (IPMA) for weather forecasting, and represents the typical weather conditions in the Metropolitan Area of the Porto region. Table 1 shows the four variables used in this research, the sensors and respective ranges and accuracies.

The temperature ($T_{ext}$) and solar radiation (GSR) sensors are installed at 1.5 m from the ground, while the wind speed ($V_{10}$) and direction (WD) are measured at 10.0 m from the ground. The analysis was carried out using the 10-min interval data collected between the January 1, 2015 and the December 31, 2015. This corresponds to the shorter time step usually available at the meteorological weather stations that make up the national network of IPMA (Portuguese Institute for Sea and Atmosphere). A shorter time step would allow one to even more accurately observe the wind speed and direction changes, still a compromise between the available datasets and the computing capacity must be made.

**Table 1**
Variables and sensors characteristics at the weather station.

| Variable | Sensor | Range | Accuracy |
|---|---|---|---|
| $T_{ext}$ | Vaisala HMP155 | −80 … +60 °C | ±0.2 °C |
| $V_{10}$ | Vaisala WAA15A | 0.4 … 60 m/s | ±0.17 m/s |
| WD | Vaisala WAV15A | 0 … 360° | ±3.0° |
| GSR | Kipp & Zonen CM11 | 0 … 1400 W/m2 | ±3.0% |

For the specific goals of this research, four setups (AveT, ReaT, ReaTM, DisTM) were established, each defining different approaches to combine meteorological data and meteorological variability. The order of the setups intends to isolate and portray the effect of accrued complexity. Fig. 2 provides a flowchart of the complete methodology, including the different pre-processing steps required by each setup.

The AveT setup considers hourly averaged meteorological data. The second setup, ReaT, differs from the previous by using the 10-min readings in the meteorological data. The wind shear coefficients in both setups are based only on terrain features. In other words, the atmospheric stability is assumed as neutral. The comparison of these two setups allows one to perceive the effect of the time step.

The third setup, ReaTM, differs from ReaT by considering the variability in the meteorological component required to quantify the wind shear coefficients. The comparison of the two setups exposes the importance of considering variable atmospheric stability conditions.

In the last setup, DisTM, a stochastic approach is implemented to consider the meteorological variability. To that end, hourly distributions of all the meteorological input variables are included in the simulation. The comparison between DisTM and ReaTM shows the effect of considering stochastic meteorological inputs.

The stochastic analysis implemented in DisTM requires the definition of hourly probability density functions (PDFs). Despite, in larger time frames, wind speed commonly following Weibull distributions [42], and air temperatures following distributions close to normal [43], one understands that for lower time frames, such as 1 h time steps, the probability of events can be assumed as constant. Therefore, the hourly distributions for exterior air temperature, wind direction, and wind speed at 10 m of height are considered as uniform.

The pseudo-random numbers from the assumed uniform

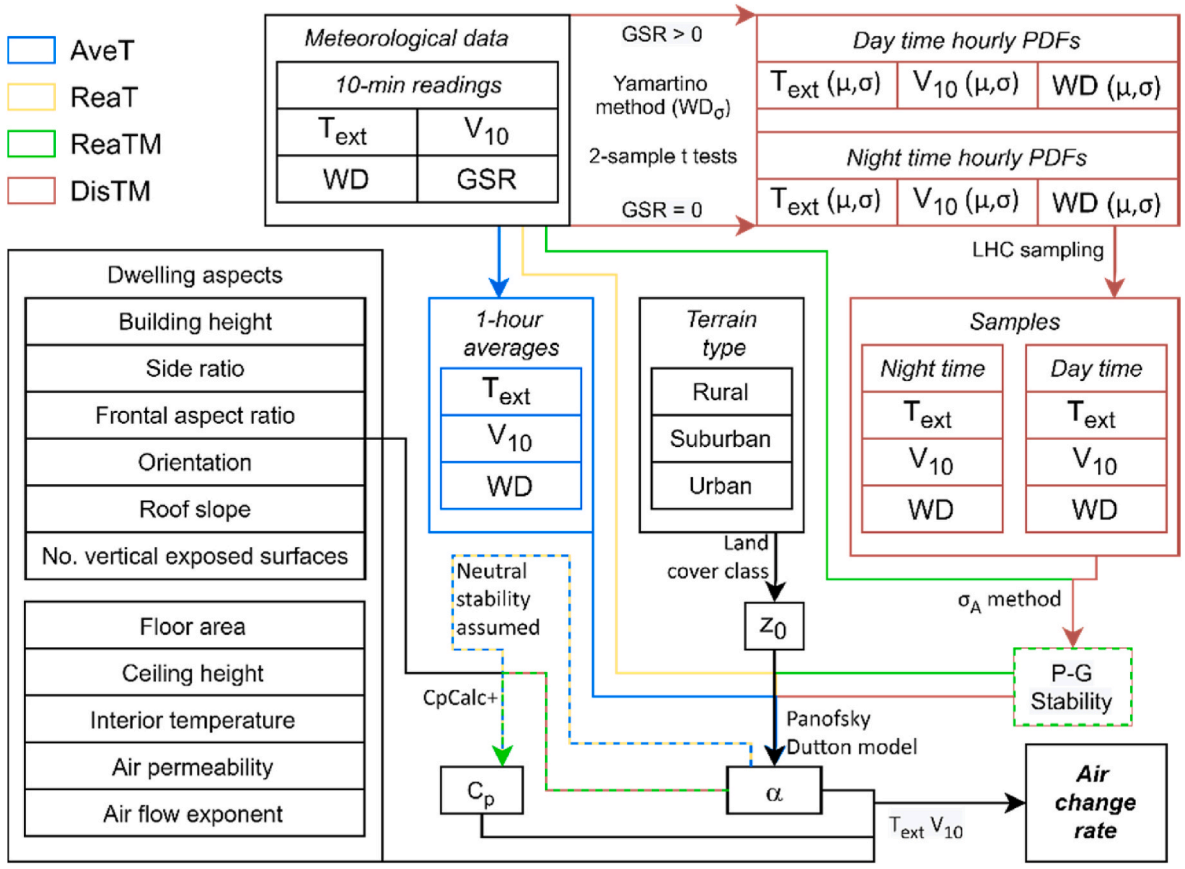


**Fig. 2.** Flowchart of the methodology.

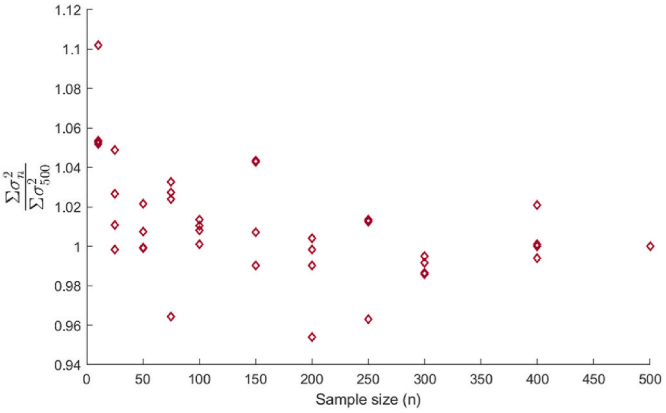


**Fig. 3.** Variance of meteorological variables as a function of sample size normalized to the variance of the maximum tested sample size.

distributions are then obtained through Latin Hypercube (LHC) sampling, using the Mersenne Twister generator with a fixed seed. A correlation matrix between Text, WD, and V10 is inputted in the sampling process for each hour.

Fig. 3 provides data on this regard for 4 h with exceptionally high variability. The sample size was set to 50 elements, at which no hour exceeded the variability of a 500 elements sample in more than 2.15%.

To obtain the standard deviation of the wind direction, also required for the DisTM setup, the Yamartino method is used [44,45] (Eqs. 9–12).

$$\sigma_A = \sigma_{WD} = \arcsin(\varepsilon)\left[1 + \left(\frac{2}{\sqrt{3}} - 1\right)\varepsilon^3\right]\frac{180}{\pi} \tag{9}$$

$$\varepsilon = \sqrt{1 - \left(s_a^2 + c_a^2\right)} \tag{10}$$

$$s_a = \frac{1}{6}\sum_{i=1}^{6} sin\theta_i \tag{11}$$

$$c_a = \frac{1}{6}\sum_{i=1}^{6} cos\theta_i \tag{12}$$

Afterwards, to classify the atmospheric stability, the hours must be classified into daytime or nighttime. The GSR value is used to that end: positive values correspond to day time, while null values are night time. This distinction further affects the way the applied $\sigma_A$ method estimates the Pasquill-Gifford (P-G) stability classes [46]. The $\sigma_A$ method is a lateral turbulence method, which uses as inputs the scalar mean wind speed ($V_{10}$) in combination with the standard deviation of the horizontal component of the wind direction ($WD_\sigma$) [47].

From the available models used for wind speed extrapolation, the Panofsky Dutton (PD) model [48] was chosen as it shows one of the highest accuracies [49,50]. This model uses the power law equation, Irwin approximations of atmospheric stability and stability length to calculate wind shear coefficients [16]. The power law in wind vertical profiles is an approximation of the logarithmic law, but because true profiles are often too complex because of non-uniform terrain, the first is seen as an acceptable approximation of the latter, and therefore is often applied in engineering practice [48]. More recent research supports this approach [51,52]. Stability length is based on the surface roughness ($z_0$) [53] and curve-fitting constants on stability classes [54].

A surface roughness of 0.1 was considered, corresponding to an exposed building, in line with the surface roughness at the weather station site and Corine Land Cover (CLC) classification [55].

The CpCalc+ [23] software is used to output wind pressure

coefficients. An entire collection of wind pressure coefficients is calculated for each wind shear coefficient associated with each atmospheric stability class. In CpCalc + each surface is discretized by a 10 × 10 points mesh equally spaced. Subsequent averaging is done for inclusion in the air infiltration balance. The wind shear coefficients were limited to the range 0.1–0.4 since these are the confidence limits defined in CpCalc+. The values were calculated for angle steps of 45°, and a linear interpolation within each 45° was assumed to obtain the 1° step values for the 360 possible angles.

Still, there are still some important issues that must be taken into account and that prevent the generalization of this methodology in the present state of air infiltration research:

- the category boundaries of $\sigma_A$ method require adjustments according to the site roughness, and the roughness length is typically not uniform in all directions at the measuring site;
- while CpCalc + provides an interesting tool to obtain the wind pressure coefficients with changing wind shear coefficient, its use is limited to some predefined standard geometries and to specific ranges of wind shear coefficients (particularly the upper limit cap).

### 2.3. Case study

To showcase the proposed objectives, a low-rise building representative of the Portuguese built stock was considered. The number of floors, floor area and ceiling height are the average of a dataset of reference buildings used in previous studies [56,57]. The case study has two floors, a floor area of 126.5 $m^2$ and a ceiling height of 2.63 m. The side ratio is 1:1, the frontal aspect ratio is 1:1, and a double pitched roof with 20° slopes is considered.

The airtightness characteristics were defined from a compilation of Portuguese studies [58–61], leading to an average $n_{50}$ of 7.60 $h^{-1}$. Since the pool of studied houses is quite limited, the whole pool of dwellings was used, amounting to 72 elements. Still, as over 96% of the Portuguese built stock is below four floors [62], and low-rise buildings are taken as those with less than 15 m height above ground, the present approach is deemed acceptable.

As the adoption of a specific air leakage configuration was not relevant for the study, the generic scenario of uniformly distributed air permeability was adopted, a typical routine in cases where a whole building blower door test is performed. However, as the envelope of the case study is quite leaky, common of southern European built stocks, it would be relevant to research case studies with identified main air leakage paths to compare with the results from the present work hypothesis of uniform air leakage path distribution.

Because the side ratio is of 1:1, all vertical surfaces are exposed, and the roof slope is of 20°, the envelope area yields approximately 234 $m^2$, and the conversion to $q_{50}$ results in 10.8 $m^3/h{\cdot}m^2$.

The airflow coefficient (C) is weighted according to the contribution of each exposed surface. Since the side ratio is 1:1, 10.52 $m^3h^{-1}Pa^{-n}$ is attributed to each split of vertical envelope surface areas in each floor, and each half of the roof represents 34.05 $m^3h^{-1}Pa^{-n}$. The airflow exponent was considered to be 0.67, corresponding to a combination of laminar and turbulent flows [63], as recommended by ASHRAE [41] when measurement data is not available.

Two vertical ducts were considered, one per floor. Their pressure drop was defined as medium, proper of ducts with diameters between 125 mm and 200 mm and a free flow area equal to or higher than 70%. With these characteristics, the airflow coefficient is equal to $44.2/(1.93 + 0.14\ L)^{0.5}$, where L is the length of the vertical duct [64]. The airflow exponent (n) for these elements is 0.5 [65].

As it is expected that the occupants strive for thermal comfort, the interior temperature was modelled based on the adaptive method proposed in EN 16798-1:2019 [66] for thermal comfort in free-running buildings.

The heating season was considered to be from the 1st day of October to the 30th day of April, in line with the Portuguese regulation for the buildings energy efficiency [67]. During this period, when the exponentially weighted running mean of the daily mean external air temperature ($T_{rm}$) is above 10 °C, the interior temperature is considered to be 19 °C. When $T_{rm}$ goes below 10 °C, the interior temperature is considered to be 18 °C.

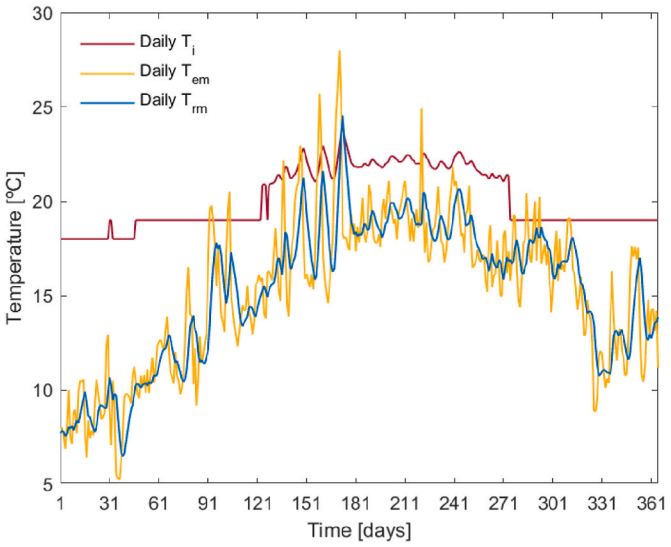


**Fig. 4.** Daily mean interior temperature ($T_i$), mean exterior temperature ($T_{em}$), and running mean exterior temperature ($T_{rm}$), for the whole year.

In the cooling season, the interior temperature is $T_i = 0.33T_{rm}+18.8–3$, corresponding to the lower limit of Category II of acceptability. Fig. 4 portrays these temperatures daily for the whole year.

## 3. Results and discussion

### 3.1. Whole year analysis of the ACH

The descriptive statistics on the ACH results obtained for the whole year in each setup is presented in Table 2. The differences between the setups are not significant, particularly in what concerns measures of central tendency. This situation occurs because data of the whole year is being grouped and, with this procedure, relevant information ends up being lost. These results highlight the importance of considering the intra-hour variability if one intends to perceive the variations between the outputs of the setups.

### 3.2. Time step effect

This subsection presents the results of the comparison between AveT and ReaT setups. These two setups assume neutral conditions, corresponding to P-G stability class D, which, when combined with a terrain roughness of 0.1 m, results in a wind shear coefficient of 0.185. Fig. 5 presents the comparison between the air change rates in the two setups for the first 72 h of the dataset.

The dots in the scatter correspond to the 10-min readings simulated in ReaT and expose the variability in the ACH values for each hour. The magnitude of this effect is randomly distributed throughout the dataset.

Regarding the whole year, Fig. 6a presents the relative differences in the calculated ACH between using the hourly averages (AveT) or the 10-min time step readings (ReaT) of the meteorological data (sample size = 52560). Fig. 6b portrays the hourly ACH standard deviations using the ReaT setup (sample size = 8760).

The relative differences in ACH distributions are nearly symmetrical, with 50% of the occurrences within −6.3% and 6.9%, between the 1st

**Table 2**
Descriptive statistics of the results of the setups for the whole year dataset.

| ACH [$h^{-1}$] | Mean | Std. Dev. | Min | 1% | 5% | 25% | Median | 75% | 95% | 99% | Max |
|---|---|---|---|---|---|---|---|---|---|---|---|
| AveT | 0.527 | 0.275 | 0.045 | 0.155 | 0.227 | 0.332 | 0.459 | 0.649 | 1.080 | 1.481 | 2.282 |
| ReaT | 0.530 | 0.282 | 0.010 | 0.142 | 0.219 | 0.332 | 0.459 | 0.653 | 1.093 | 1.516 | 2.444 |
| ReaTM | 0.517 | 0.285 | 0.010 | 0.145 | 0.218 | 0.323 | 0.436 | 0.635 | 1.093 | 1.516 | 2.444 |
| DisTM | 0.517 | 0.285 | 0.003 | 0.146 | 0.218 | 0.322 | 0.435 | 0.633 | 1.093 | 1.515 | 2.440 |

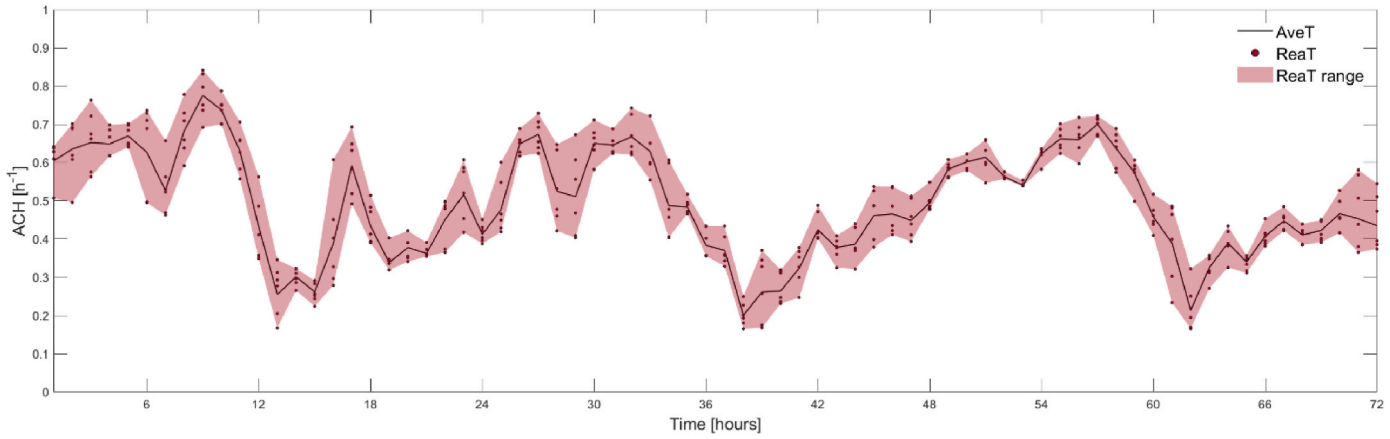


**Fig. 5.** Air change rates (ACH) in AveT and ReaT setups from the 1st to the 3rd of January.

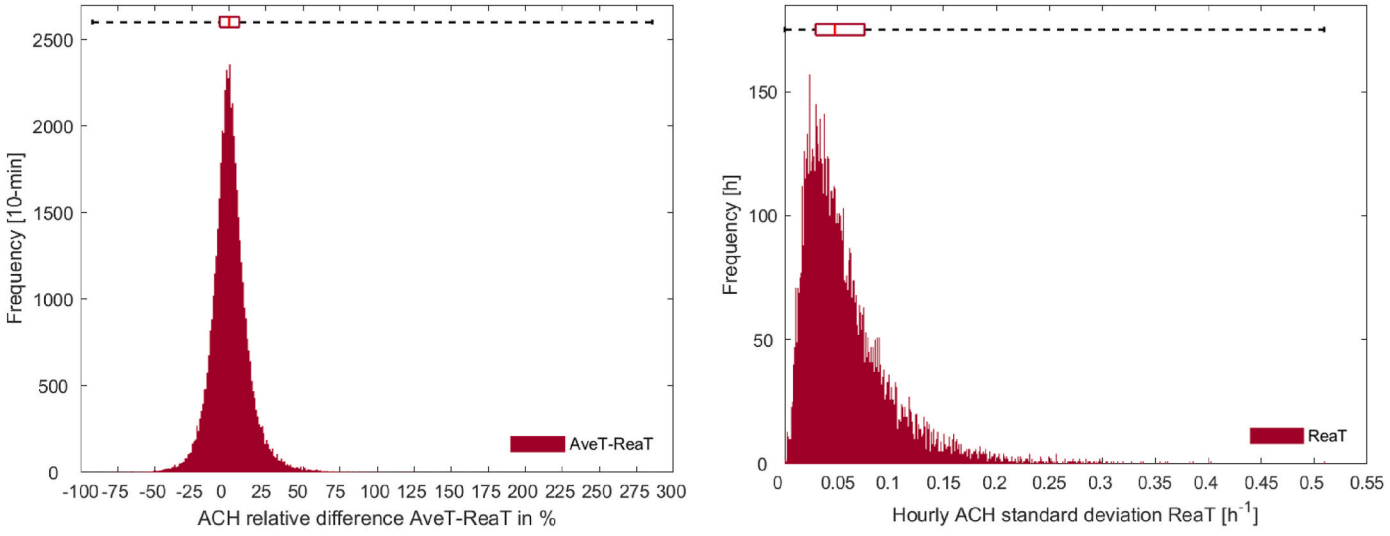


**Fig. 6.** Comparison between AveT and ReaT setups: a) air change rates (ACH) relative difference; b) hourly air change rates (ACH) standard deviation in ReaT setup.

**Table 3**
Whole year occurrences of P-G stability classes in ReaTM setup and their effect over wind shear coefficients (WSCs) and wind pressure coefficients (WPCs) (terrain roughness of 0.1 m).

| P-G stability | Occurrences | WSC [−] | Cp1L [−] | Cp1U [−] |
|---|---|---|---|---|
| A | 2507 | 0.104 | 0.655 | 0.755 |
| B | 1394 | 0.112 | 0.653 | 0.746 |
| C | 2802 | 0.131 | 0.643 | 0.723 |
| D | 30204 | 0.185 | 0.594 | 0.661 |
| E | 10130 | 0.344 | 0.261 | 0.473 |
| F | 5523 | 0.591 | 0.078 | 0.403 |

and 3rd quartiles. However, differences below −18.6% and above 22.5% can be found at the 5% and 95% quantiles. Observing Figs. 6b and 50% of the hours throughout the year have standard deviations between 0.025 and 0.065 $h^{-1}$, corresponding to the range of the 25% quantile to the 75% quantile. The median standard deviation is of 0.040 $h^{-1}$. At the 95% quantile, the standard deviation reaches 0.126 $h^{-1}$.

### 3.3. Atmospheric stability effect

The introduction of variable atmospheric stability conditions produces changes in the calculation of the WSCs and consequently in the WPCs. While AveT and ReaT consider unchanging neutral conditions, in ReaTM and DisTM one of the following situations of the P-G stability

**Table 4**
Descriptive statistics of the relative differences between ReaT-ReaTM setups.

| Δ ACH | Mean | Std. Dev. | Min | 0.01 | 0.05 | 0.25 | Median | 0.75 | 0.95 | 0.99 | Max |
|---|---|---|---|---|---|---|---|---|---|---|---|
| ReaT-ReaTM [%] | −4.4 | 22.1 | −71.9 | −45.8 | −34.6 | −18 | −8.5 | 8.2 | 37.4 | 59.2 | 122.7 |
| ReaT-ReaTM [$h^{-1}$] | −0.031 | 0.095 | −0.361 | −0.27 | −0.202 | −0.082 | −0.029 | 0.023 | 0.131 | 0.207 | 0.31 |

classification can occur: unstable conditions (classes A, B and C); neutral conditions (class D); or stable conditions (classes E and F). To isolate the effect of considering a variable atmospheric stability classification, only the results of ReaT and ReaTM are showed in this subsection.

Table 3 exposes the effect of the consideration of the meteorological variability in the computation of WSCs and WPCs. For example, WPCs of the windward vertical exposed wall, for a wind angle incidence of 0°, are presented: Cp1L refers to the lower floor, and Cp1U to the upper floor.

Neutral conditions (class D) are the most common and occur 57.47% of the time, while unstable atmosphere occurs in 12.75% (classes A, B and C), and the remaining 29.78% correspond to stable conditions (classes E and F). When the atmospheric stability tends to unstable conditions, the reduction of wind speed with height is less pronounced, and therefore the WSCs decrease when unstable conditions are present. Reversely, in stable atmospheric conditions, the wind effect is minored as the vertical reduction of wind speed is more drastic, and therefore higher WSCs occur. This effect is reflected in the WPCs. As the wind effect loses relevance, from unstable to stable atmospheric stability conditions, the WPCs experience a progressive reduction.

Since the difference between ReaT and ReaTM is the consideration of atmospheric stability classes other than neutral, when comparing both setups, the differences lie in the group of the non-neutral occurrences, which in this case were 42.53% of the total. A descriptive statistic of the differences found in the non-neutral occurrences is presented in Table 4.

As the mean of the ACH differences tend to negative values (−0.031 $h^{-1}$), it indicates that the entire year's atmospheric stability skews for stable conditions in the studied location. The standard deviation is 0.095 $h^{-1,}$ and the differences ranged between −0.20 and + 0.13, 5 and 95% quantiles, respectively.

Fig. 7 informs on these impacts. Hour zero corresponds to midnight on the 1st of January. During the nighttime, the ACH in ReaTM are consistently lower than in ReaT, with stable conditions predominant (blue rectangle). During the daytime, unstable atmospheric conditions result in higher ACH in ReaTM (red rectangle). When neutral conditions occur during an entire hour, the ranges of ReaTM and ReaT overlap (green rectangle).

Another interesting finding, that can be spotted in Fig. 7, is that generally, neutral conditions are more sensitive to the time step effect than stable conditions, as for those hours, the readings experience greater dispersion (blue rectangle). On the other hand, the atmospheric stability effect tends to gain significance over the time step effect for more modest wind speeds, when unstable conditions are present (red rectangle).

These effects are observed in the pressure differences across the parametrized surfaces, for hours 34 (Fig. 8a) and 52 (Fig. 8b), representing unstable and stable atmospheric stabilities, in ReaTM, respectively. For referencing, the surface nomenclature can be consulted in Fig. 1 and in the paragraph immediately after it.

From neutral to unstable conditions, the wind shear coefficient gets smaller, therefore increasing the wind pressure coefficients, resulting in increments in the occurring pressure differences across the envelope (Fig. 8a). From neutral to stable conditions, the greater wind shear coefficient, develops decreasing wind pressure coefficients, which reflects the decline in the occurring pressure differences across the surfaces of the envelope (Fig. 8b). Fig. 9 reports on ACH differences in ReaT-ReaTM, for the occurrences classified as non-neutral in the latter (sample size = 22353) and divided by stability class for the whole year.

In some occurrences the ACH from neutral to stable conditions increases and decreases from neutral to unstable conditions. In all these occurrences, the exterior temperature is higher than the interior temperature. Therefore, the stack effect is countering the wind effect ascendant movement, resulting in partial or total vertical flow inversion. With this rationale, one understands that by locking one of the effects and steadily increasing the other, it withers until the forces cancel each other before the ACH grows.

### 3.4. Stochastic modelling effect

Fig. 10 portrays the effect of introducing a stochastic nature in the input data using the 1st to the 3rd of January as an example. As can be seen, the DisTM setup results in wider hourly ACH ranges for the majority of the hours.

As expected, the effect of the stochastic modelling of the meteorological variables does not significantly affect the P-G classification since a significant difference would indicate a distortion from reality. The most substantial changes from ReaTM to DisTM occur in class D with a decrease of 0.24%, and in class F with an increase of 0.19% (Fig. 11a). The minor differences found give robustness to the application of

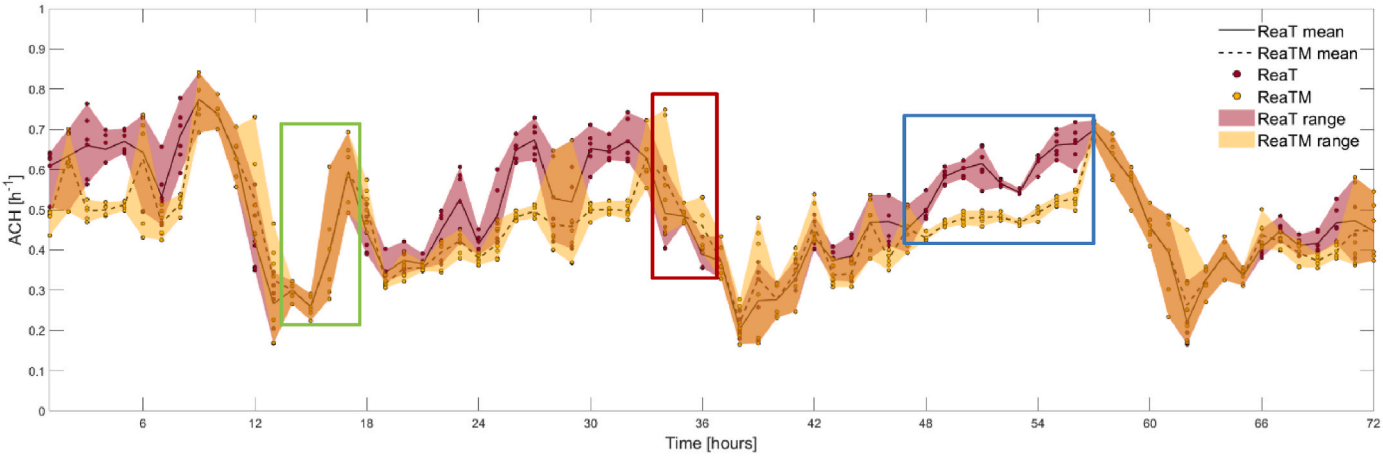


**Fig. 7.** Average air change rates (ACH) and respective confidence bands in the ReaT and ReaTM setups from the 1st to the 3rd of January of the meteorological dataset.

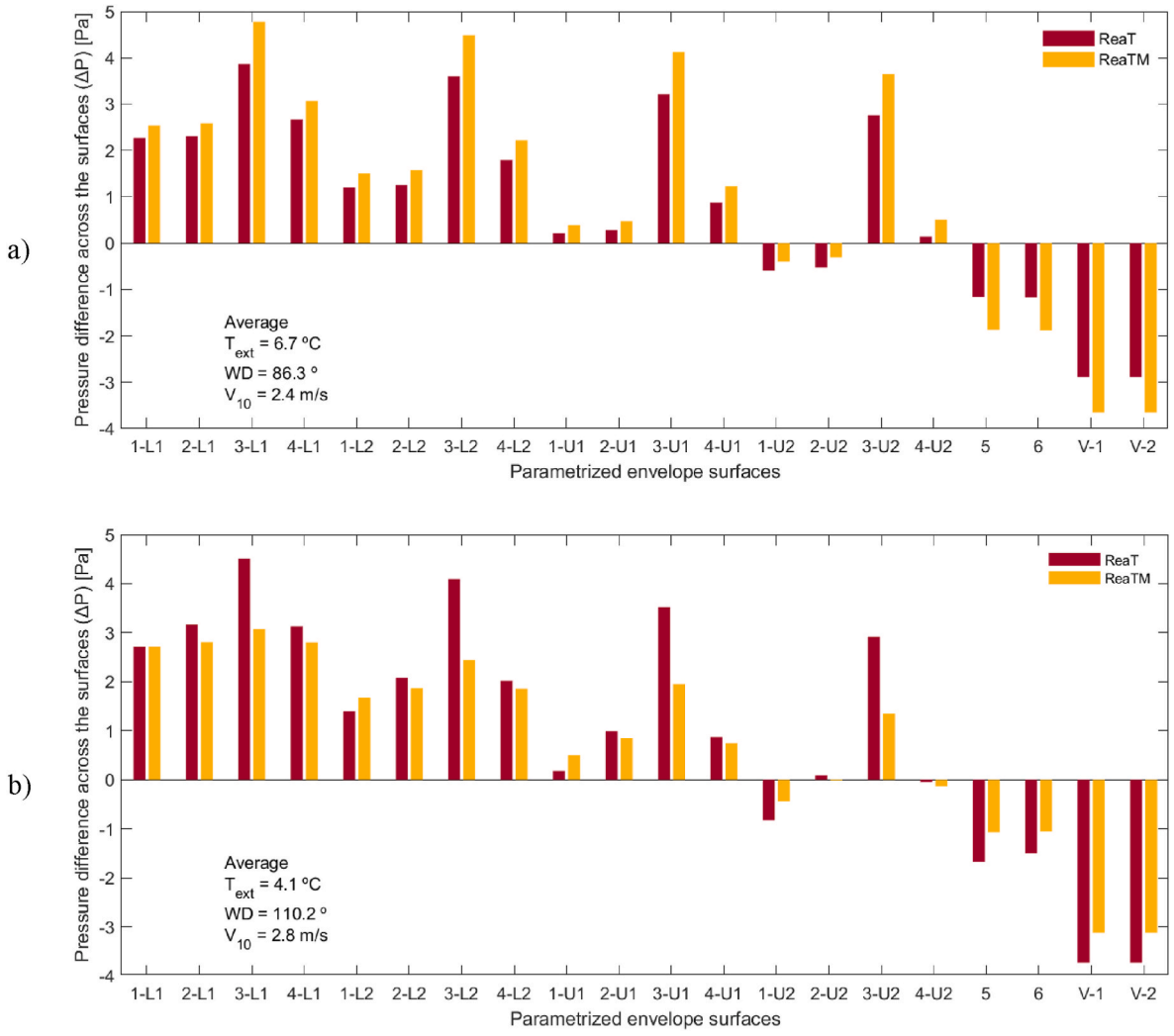


**Fig. 8.** Pressure differences across the parametrized envelope surfaces for specific hours in the ReaT and ReaTM setups: a) hour 34 in class C, unstable conditions; b) hour 52 in class E, stable conditions. ReaT represents static class D, neutral conditions.

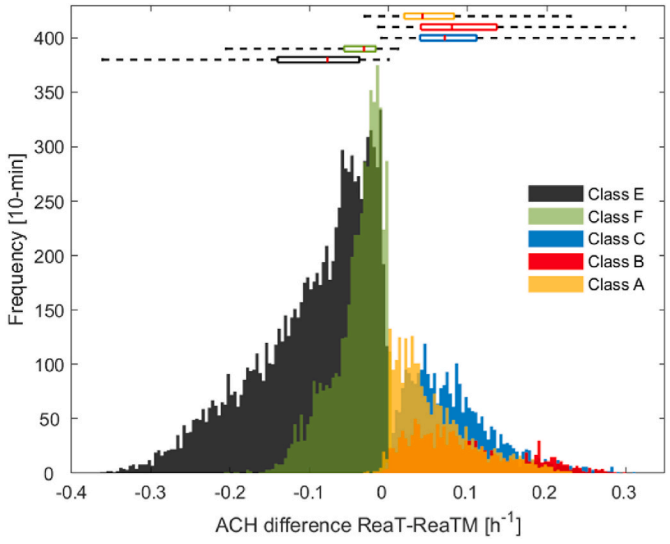


**Fig. 9.** Air change rates (ACH) differences between ReaT-ReaTM setups for the readings classified with non-neutral atmospheric stability.

uniform distributions to the meteorological variables.

The comparison between ACH in ReaTM and DisTM by location measures is inappropriate since the aim is to consider additional possible intra-hourly occurring phenomena. As Fig. 11b shows, the use of hourly uniform distributions confers a rather lognormal distribution of the relative differences in ACH ranges. The median of the relative differences between the two setups increased 19.6%, while the mean increased 29.3%.

Still, a percentage of the hours in DisTM results in narrower outputted ACH ranges than in ReaTM (14.3%). Details on two particular hours are presented in Fig. 12, representing the advantages and limitations of the consideration of hourly distributions. Cp1 refers to the windward wall, Cp2 to the opposite leeward wall. Cp3 and Cp4 refer to the lateral walls. The L and U refer to the lower floor and upper floor, respectively.

Fig. 12a shows that the existence of a reading far from the others results in the assumed uniform distribution not including it. While, for Cp1, Cp2, and Cp4, the range of DisTM is more comprehensive than that of ReaT, for Cp3 the range of DisTM is one-third of that of ReaT.

Fig. 12b portrays the advantage of using the uniform distributions, as the sampled meteorological values result in wind pressure coefficients along, between, and slightly over the ReaT readings range. As these represent over 86.6% of the hours in the whole studied year, it seems a reasonable trade-off.

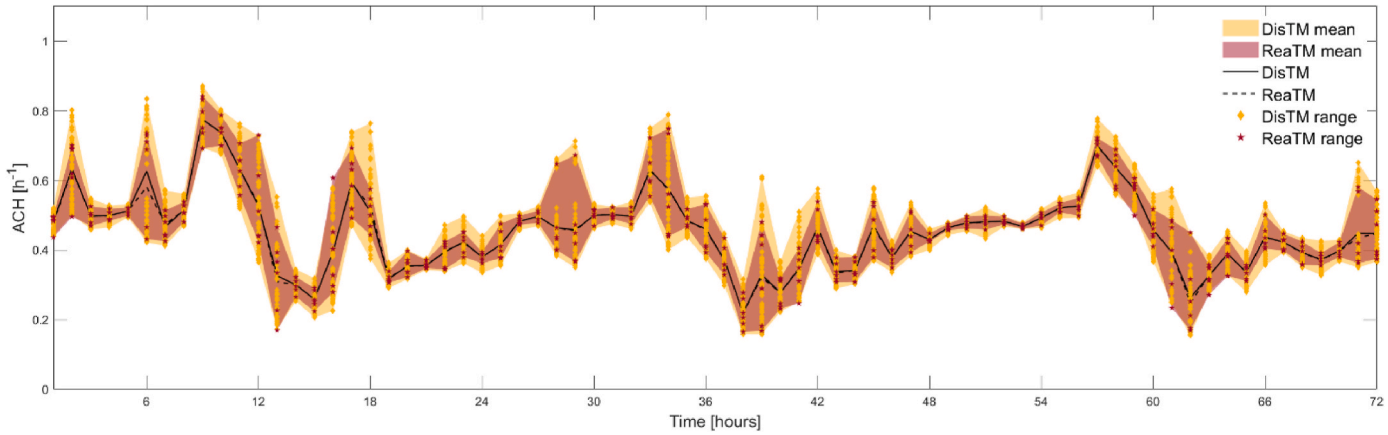


**Fig. 10.** Air change rates (ACH) ranges, averages and scatters in the ReaTM and DisTM setups from the 1st to the 3rd of January of the used meteorological dataset.

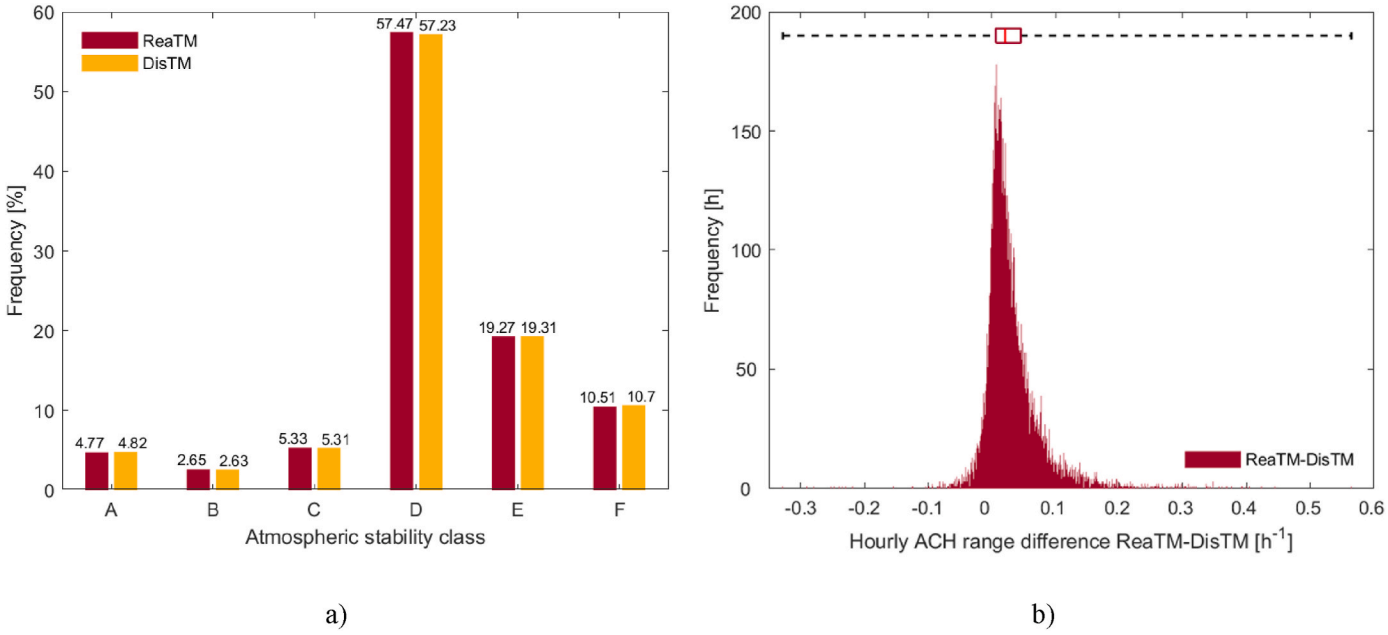


**Fig. 11.** Comparisons between ReaTM and DisTM setups: a) occurrence of Pasquill-Gifford (P–G) stability classes; b) hourly air change rates (ACH) range difference.

### 3.5. Combined effect

The step-wise increment in complexity from one setup to the following made it possible to single out the impact of each effect in the intra-hour dispersion of the air change rates. Comparing the outputted ACH of the first setup, AveT, with the full proposed methodology, DisTM, highlights the full scope of the disparities. Fig. 13 shows for the first 72 h of the dataset the hourly averages resulting from the AveT setup and the hourly averages and ranges resulting from the DisTM setup. Significant differences are observed between the averages of the two setups, with DisTM consistently outputting lower ACH during nighttime and higher in daytime periods.

## 4. Conclusions

The work presented intended to evaluate the effect of atmospheric stability and intra-hour variability of meteorological variables in quantifying air change rates in buildings with natural ventilation and leaky envelopes. The following conclusions can be drawn:

- Using 10-min readings instead of hourly meteorological data in ACH simulations detected a time step effect showed, in this case study, by an hourly standard deviation of ACH between 0.025 and 0.065 $h^{-1}$ (between the 25% and 75% quantiles) while at the 95% quantile the standard deviations reached 0.126 $h^{-1}$;
- Atmospheric stability classes showed to change outputted results significantly. Non-neutral conditions were recorded in approximately 43% of the time. The hourly ACH relative differences between a setup with neutral atmospheric conditions and another setup where varying atmospheric conditions are admitted averaged $-0.031$ $h^{-1}$, with a standard deviation of 0.095 $h^{-1}$. At the 5% and 95% quantiles, the ACHs differences were $-0.202$ $h^{-1}$ and 0.131 $h^{-1}$, respectively.
- The similar results found for the atmospheric stability classification when using deterministic vs. stochastic meteorological variability gives robustness to the application of hourly uniform distributions to the meteorological variables considered;
- From deterministic to stochastic meteorological variability, the average ACH range increased by an average of 29.3%. Still, in 13.4% of the events the hourly ACH ranges were narrower in the stochastic

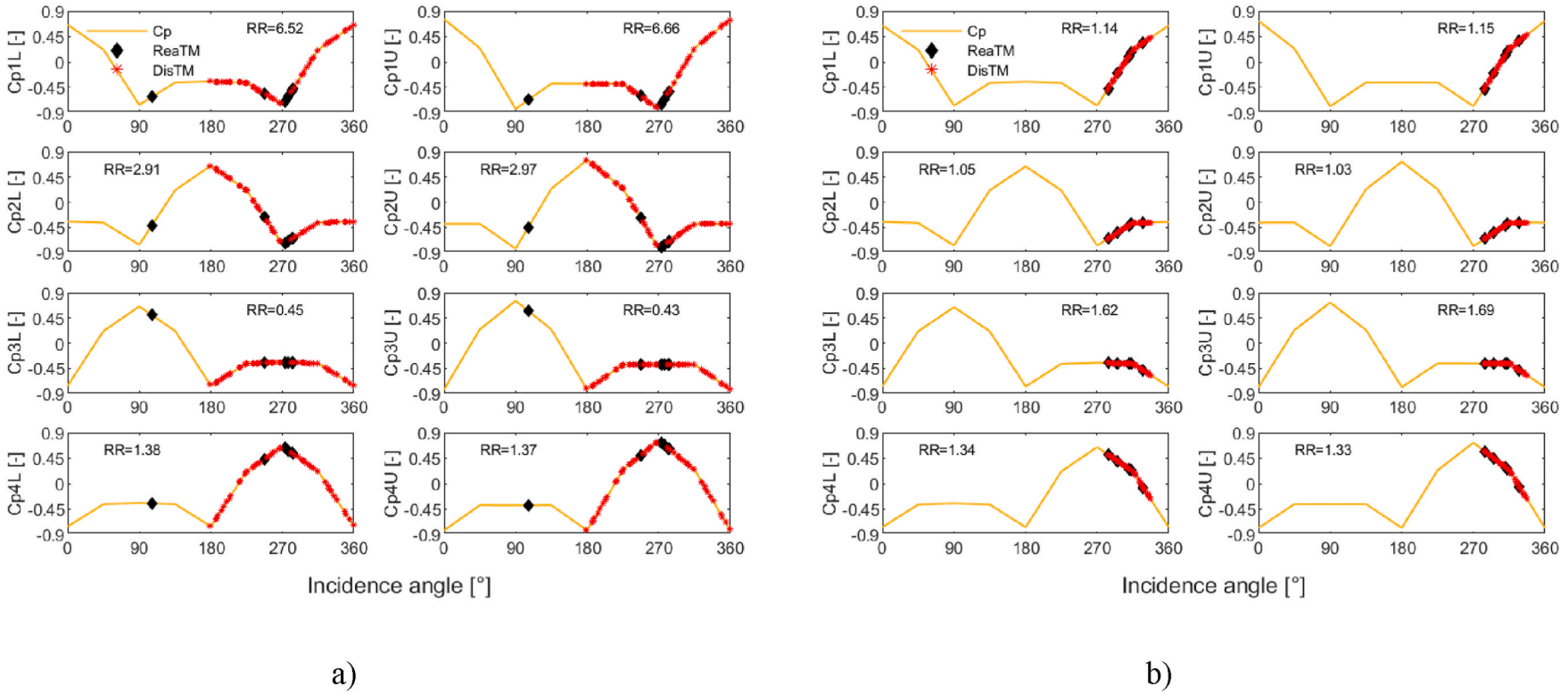


**Fig. 12.** Comparison of wind pressure coefficients (WPCs) of the vertical exposed surfaces for ReaTM and DisTM setups in the hour 160 (a) and hour 138 (b) of the used meteorological dataset; RR refers to range ratio.

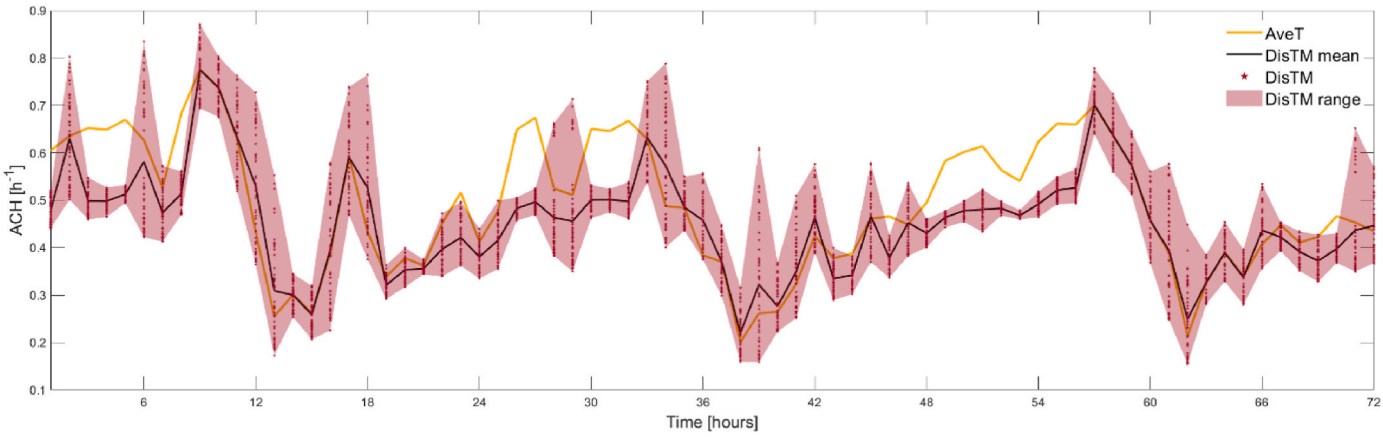


**Fig. 13.** Average air change rates (ACH) in AveT and DisTM setups, range band and scatter in DisTM from the 1st to the 3rd of January of the meteorological dataset.

simulation setup. This is due to the limitation of the hourly uniform distributions in encompassing all the 10-min readings of these hours.

The methodology detailed and discussed in this work considers shorter time steps and the effect of changing atmospheric stability to evaluate the fluctuations in environmental conditions that influence infiltration driven air change rates in building envelopes. Using hourly distributions and stochastic sampling ensures that the values in between and others potentially occurring around the boundaries are being considered for ACH calculation, therefore providing a more exhaustive approximation of the actual conditions.

While for a year-long joint observation, these findings do not significantly change the central tendency of the ACH, they provide important information on the intra-hour dispersion, which can be helpful to better predict hourly ranges of performance that can have multiple applications in the ventilation strategy, either in the design stage or in the optimization of the performance of an existing building.

The future generalization of the methodology includes the definition of additional combinations of building geometries and terrain roughness, assessing the impact on results of using alternative formulations, such as the quadratic equation in modelling airflow paths, and the logarithmic law in vertically extrapolating wind speeds, and analyzing the correlation between meteorological variables and pressure distribution along the building facade.

Future works are undergoing regarding the correlation between meteorological variables and building and terrain variables and their importance in explaining the variability of the outputted air change rates. One considers these relationships better suited to be addressed in these futures works since their methodology considers a wider variability of dwelling features.

## Declaration of competing interest

The authors declare that they have no known competing financial interests or personal relationships that could have appeared to influence the work reported in this paper.

## Acknowledgments

This work was financially supported by: Base Funding - UIDB/04708/2020 and Programmatic Funding - UIDP/04708/2020 of the CONSTRUCT - Instituto de I&D em Estruturas e Construções - funded by national funds through the FCT/MCTES (PIDDAC). The author would like to acknowledge the support of FCT - Fundaçaõ para a Cieˆncia e a Tecnologia, the funding of the Doctoral Grant PD/BD/135162/2017, through the Doctoral Programme EcoCoRe.

The authors also acknowledge Dr. Ricardo Deus and the Portuguese Institute for Sea and Atmosphere, I. P. (IPMA, IP) for providing the meteorological dataset for this work.

## References

[1] K. Engeland, M. Borga, J.-D. Creutin, B. François, M.-H. Ramos, J.-P. Vidal, Space-time variability of climate variables and intermittent renewable electricity production – a review, Renew. Sustain. Energy Rev. 79 (2017) 600–617.
[2] R. Marquez, C.F.M. Coimbra, Intra-hour DNI forecasting based on cloud tracking image analysis, Sol. Energy 91 (2013) 327–336.
[3] M. Koivisto, G.M. Jónsdóttir, P. Sørensen, K. Plakas, N. Cutululis, Combination of meteorological reanalysis data and stochastic simulation for modelling wind generation variability, Renew. Energy 159 (2020) 991–999.
[4] D.B. Crawley, J.W. Hand, M. Kummert, B.T. Griffith, Contrasting the capabilities of building energy performance simulation programs, Build. Environ. 43 (4) (2008) 661–673.
[5] H.B. Awbi, in: Ventilation of Buildings, second ed., Taylor & Francis, Philadelphia, PA, USA, 2003.
[6] Y. Al horr, M. Arif, M. Katafygiotou, A. Mazroei, A. Kaushik, E. Elsarrag, Impact of indoor environmental quality on occupant well-being and comfort: a review of the literature, Int. J. Sustain. Built Environ. 5 (1) (2016) 1–11.
[7] J. Langmans, T.Z. Desta, L. Alderweireldt, S. Roels, Durability of self-adhesive tapes for exterior air barrier applications : a laboratory investigation, Int. J. Vent. 3315 (2017).
[8] W. Bracke, J. Laverge, N. Van Den Bossche, and A. Janssens, "Durability and measurement uncertainty of airtightness in extremely airtight dwellings," Int. J. Vent., vol. 14, no. 4, pp. 383–394, Mar. 2016.
[9] O. Seppänen, N. Brelih, G. Goeders, A. Litiu, "Existing Buildings, Building Codes, Ventilation Standards and Ventilation in Europe," *Final Heal*, WP5 Rep., 2012.
[10] M.W. Liddament, Air Infiltration Calculation Techniques – an Application Guide, 1986.
[11] L. Gu, Airflow network modeling in EnergyPlus," in, Building Simulation 10 (2007).
[12] W.S. Dols, S.J. Emmerich, B.J. Polidoro, Coupling the multizone airflow and contaminant transport software CONTAM with EnergyPlus using co-simulation," in, Building simulation 9 (4) (2016) 469–479.
[13] F. Haghighat, A comprehensive validation of two airflow models - COMIS and CONTAM, Indoor Air 6 (4) (1996) 278–288.
[14] F. Haghighat, J. Rao, P. Fazio, The influence of turbulent wind on air change rates—a modelling approach, Build. Environ. 26 (2) (1991) 95–109.
[15] D. Kraniotis, Dynamic characteristics of wind-driven air infiltration in buildings the impact of wind gusts under unsteady wind conditions, PhD thesis, Nor. Univ. Life Sci. PhD thesis (2014) 44–48, https://doi.org/10.13140/RG.2.1.3607.9444.
[16] J.S. Irwin, A theoretical variation of the wind profile power-law exponent as a function of surface roughness and stability, Atmos. Environ. 13 (1) (1979) 191–194.
[17] G. Gualtieri, Atmospheric stability varying wind shear coefficients to improve wind resource extrapolation: a temporal analysis, Renew. Energy 87 (2016) 376–390.
[18] I. Walker, D. Wilson, AIM 2: the Alberta Air Infiltration Model, 1990.
[19] R.N. Farrugia, The wind shear exponent in a Mediterranean island climate, Renew. Energy 28 (4) (2003) 647–653.
[20] H. Kikumoto, R. Ooka, H. Sugawara, J. Lim, Observational study of power-law approximation of wind profiles within an urban boundary layer for various wind conditions, J. Wind Eng. Ind. Aerod. 164 (2017) 13–21.
[21] J. Lim, Y. Akashi, R. Ooka, H. Kikumoto, Y. Choi, A probabilistic approach to the energy-saving potential of natural ventilation: effect of approximation method for approaching wind velocity, Build. Environ. 122 (2017) 94–104.
[22] J. Lim, R. Ooka, H. Kikumoto, Effect of diurnal variation in wind velocity profiles on ventilation performance estimates, Energy Build. 130 (2016) 397–407.

[23] M. Grosso, Wind pressure distribution around buildings: a parametrical model, Energy Build. 18 (2) (1992) 101–131.
[24] H. Breesch, A. Janssens, Performance evaluation of passive cooling in office buildings based on uncertainty and sensitivity analysis, Sol. Energy 84 (8) (2010) 1453–1467.
[25] D. Cóstola, B. Blocken, J.L.M. Hensen, Overview of pressure coefficient data in building energy simulation and airflow network programs, Build. Environ. 44 (10) (2009) 2027–2036.
[26] A.J. Bowen, A wind tunnel investigation using simple building models to obtain mean surface wind pressure coefficients for air infiltration estimates, Aero. Estab. Tech. Rep. LPR-LA- 209 (1976).
[27] S. Charisi, T. Thiis, and T. Aurlien, "Full-scale measurements of wind-pressure coefficients in twin medium-rise buildings," Buildings, vol. 9, p. 63, Mar. 2019.
[28] D. Cóstola, B. Blocken, M. Ohba, J.L.M. Hensen, Uncertainty in airflow rate calculations due to the use of surface-averaged pressure coefficients, Energy Build. 42 (6) (2010) 881–888.
[29] H. Gough, et al., Influence of neighbouring structures on building façade pressures: comparison between full-scale, wind-tunnel, CFD and practitioner guidelines, J. Wind Eng. Ind. Aerod. 189 (2019) 22–33.
[30] B.G. Wiren, Effects of surrounding buildings on wind pressure distributions and ventilative heat losses for a single-family house, J. Wind Eng. Ind. Aerod. 15 (1–3) (1983) 15–26.
[31] M. V Swami, S. Chandra, Correlations for pressure distribution on buildings and calculation of natural-ventilation airflow, Build. Eng. 94 (3112) (1988) 243–266.
[32] A. Hagos, F. Habte, A.G. Chowdhury, D. Yeo, Comparisons of two wind tunnel pressure databases and partial validation against full-scale measurements, J. Struct. Eng. 140 (10) (2014) 4014065.
[33] R.T. Muehleisen, S. Patrizi, A new parametric equation for the wind pressure coefficient for low-rise buildings, Energy Build. 57 (2013) 245–249.
[34] F. Bre, J.M. Gimenez, V.D. Fachinotti, Prediction of wind pressure coefficients on building surfaces using artificial neural networks, Energy Build. 158 (2018) 1429–1441.
[35] G. Hu, L. Liu, D. Tao, J. Song, K.T. Tse, K.C.S. Kwok, Deep learning-based investigation of wind pressures on tall building under interference effects, J. Wind Eng. Ind. Aerod. 201 (2020) 104138.
[36] M. Orme, M. Liddament, A. Wilson, Numerical Data for Air Infiltration and Natural Ventilation Calculations, 1998.
[37] CEN, Ventilation for Buildings - Calculation Methods for the Determination of Air Flow Rates in Buildings Including Infiltration. (EN 15242-2007), 2007.
[38] CEN, EN 16798-7:2017 Energy Performance of Buildings - Ventilation for Buildings - Part 7: Calculation Methods for the Determination of Air Flow Rates in Buildings Including Infiltration (Modules M5-5), 2017.
[39] M.W. Liddament, Power law rules–OK? Air Infiltration Rev. 8 (2) (1987) 4–6.
[40] I.S. Walker, D.J. Wilson, M.H. Sherman, A comparison of the power law to quadratic formulations for air infiltration calculations, Energy Build. 27 (3) (1998) 293–299.
[41] ASHRAE, ASHRAE Handbook - Fundamentals (SI Edition), American Society of Heating, Refrigerating and Air-Conditioning Engineers, Inc. (ASHRAE), 2017.
[42] J. V Seguro, T.W. Lambert, Modern estimation of the parameters of the Weibull wind speed distribution for wind energy analysis, J. Wind Eng. Ind. Aerod. 85 (1) (2000) 75–84.
[43] R.D. Harmel, C.W. Richardson, C.L. Hanson, G.L. Johnson, Evaluating the adequacy of simulating maximum and minimum daily air temperature with the normal distribution, J. Appl. Meteorol. 41 (7) (2002) 744–753.
[44] R.J. Yamartino, A comparison of several 'single-pass' estimators of the standard deviation of wind direction, J. Clim. Appl. Meteorol. 23 (9) (1984) 1362–1366.
[45] D. Bruce Turner, Comparison of three methods for calculating the standard deviation of the wind direction, J. Clim. Appl. Meteorol. 25 (5) (1986) 703–707.
[46] F. Pasquill, The estimation of the dispersion of windborne material, Met. Mag. 90 (1961) 33.
[47] D.T. Bailey, Meteorological Monitoring Guidance for Regulatory Modeling Applications, DIANE Publishing, 2000.
[48] H.A. Panofsky, Atmospheric turbulence, Model. methods Eng. Appl. 397 (1984).
[49] G. Gualtieri, A comprehensive review on wind resource extrapolation models applied in wind energy, Renew. Sustain. Energy Rev. 102 (2019) 215–233.
[50] G. Gualtieri, S. Secci, Methods to extrapolate wind resource to the turbine hub height based on power law: a 1-h wind speed vs. Weibull distribution extrapolation comparison, Renew. Energy 43 (2012) 183–200.
[51] M. Optis, A. Monahan, F.C. Bosveld, Moving beyond Monin–Obukhov similarity theory in modelling wind-speed profiles in the lower atmospheric boundary layer under stable stratification, Boundary-Layer Meteorol. 153 (3) (2014) 497–514.
[52] M.A. Lackner, A.L. Rogers, J.F. Manwell, J.G. McGowan, A new method for improved hub height mean wind speed estimates using short-term hub height data, Renew. Energy 35 (10) (2010) 2340–2347.
[53] A.G. Davenport, C. Grimmond, T. Oke, J. Wieringa, Estimating the roughness of cities and sheltered country, 15th Conf. Probab. Stat. Atmos. Sci. Conf. Appl. Climatol. Ashville, NC, Am. Meteorol. Soc. (Jan. 2000) 96–99.
[54] P. Zannetti, Air Pollution Modeling: Theories, Computational Methods and Available Software, Springer Science & Business Media, 2013.
[55] J. Silva, C. Ribeiro, R. Guedes, Roughness length classification of corine Land cover classes, in: Proceedings of the European Wind Energy Conference, Milan, Italy, vol. 710, 2007, p. 110.
[56] M. Ferreira, M. Almeida, A. Rodrigues, C. Araújo, J. Guimarães, PORTUGAL EPBD National Report on Calculation of Cost-Optimal Levels of Minimum Energy Performance Requirements for Residential Buildings, 2014.
[57] M. Ferreira, M. Almeida, A. Rodrigues, Cost-optimal energy efficiency levels are the first step in achieving cost effective renovation in residential buildings with a nearly-zero energy target, Energy Build. 133 (2016) 724–737.
[58] N.M.M. Ramos, R.M.S.F. Almeida, A. Curado, P.F. Pereira, S. Manuel, J. Maia, Airtightness and ventilation in a mild climate country rehabilitated social housing buildings – what users want and what they get, Build. Environ. 92 (2015) 97–110.
[59] R. Oliveira, A. Figueiredo, R. Vicente, R.M.S.F. Almeida, Impact of unoccupied flats on the thermal discomfort and energy demand: case of a multi-residential building, Energy Build. 209 (2020) 109704.
[60] A. Salehi, I. Torres, A. Ramos, Experimental analysis of building airtightness in traditional residential Portuguese buildings, Energy Build. 151 (2017) 198–205.
[61] A. Silva, Caracterização das infiltrações médias anuais em edifícios portugueses através do método de pressurização, Faculty of Engineering - University of Porto, 1991.
[62] INE, Statistical Information - Buildings' Tables - 2.02 - Buildings, According to the Number of Floors, by Type of Building and Number of Accommodation, 2014 [Online]. Available: https://censos.ine.pt/xportal/xmain?xpid=CENSOS&xpgid=censos_quadros_edif.
[63] ASHRAE, " Chap, 16: ventilation and infiltration, ASHRAE Handb. Fundam. (2013) 16.1–16.37.
[64] Diário República, *Despacho (extrato) n.º 15793-K/2013. D.R. n.º 234, 3.º Suplemento, Série II de 2013-12-03 Publicação dos parâmetros térmicos para o cálculo dos valores que integram o presente despacho*, 2013.
[65] C. Wray, M. Sherman, Duct Leakage Modeling in EnergyPlus and Analysis of Energy Savings from Implementing SAV with InCITeTM, Lawrence Berkeley National Lab.(LBNL), Berkeley, CA (United States), 2010.
[66] CEN, EN 16798-1:2019 Energy Performance of Buildings - Ventilation for Buildings - Part 1: Indoor Environmental Input Parameters for Design and Assessment of Energy Performance of Buildings Addressing Indoor Air Quality, Thermal Environment, Lighting and Acous, 2019.
[67] Diário República, *Despacho (extrato) n.º 15793-F/2013. D.R. n.º 234, 3º Suplemento, Série II de 2013-12-03 Publicação dos parâmetros para o zonamento climático e respetivos dados*, 2013.